Chinese Chemical Letters 35 (2024) 109631

Contents lists available at ScienceDirect

Chinese Chemical Letters

journal homepage: www.elsevier.com/locate/cclet

Se-substituted pentamethine cyanine for anticancer photodynamic therapy mediated using the hot band absorption process

Wenkai Liu[a], Yanxian Hou[a], Weijian Liu[b], Ran Wang[a], Shan He[c], Xiang Xia[a], Chengyuan Lv[a], Hua Gu[a], Qichao Yao[a], Qingze Pan[a], Zehou Su[a], Danhong Zhou[a], Wen Sun[a,*], Jiangli Fan[a,*], Xiaojun Peng[a]

[a] State Key Laboratory of Fine Chemicals, Frontiers Science Center for Smart Materials Oriented Chemical Engineering, Dalian University of Technology, Dalian 116024, China
[b] Shandong Laboratory of Yantai Advanced Materials and Green Manufacturing, Yantai 264006, China
[c] Department of Chemistry, Hong Kong Branch of Chinese National Engineering Research Center for Tissue Restoration and Reconstruction and Institute for Advanced Study, The Hong Kong University of Science and Technology, Hong Kong 999077, China

ARTICLE INFO

Article history:
Received 18 December 2023
Revised 2 February 2024
Accepted 3 February 2024
Available online 13 February 2024

Keywords:
Cyanine dyes
Hot band absorption
Anti-Stokes
Photodynamic therapy
Anticancer treatment

ABSTRACT

Photodynamic therapy (PDT) is a promising cancer treatment modality owing to its high spatiotemporal selectivity and noninvasive nature. However, conventional photosensitizers (PSs) used in PDT are responsive only to visible light, which makes them unsuitable for tissue penetration. In this study, we propose a PS based on hot band absorption (HBA), which can be triggered by anti-Stokes light at 808 nm *via* a one-photon process. The introduction of selenium (Se) into pentamethine cyanine (**Secy5**) not only facilitates intersystem crossing for reactive oxygen species (ROS) production but also enhances HBA efficiency, thereby prolonging the excitation wavelength. In addition, **Secy5** demonstrates excellent biocompatibility, unlike its I-substituted counterpart (**Icy5**), and produces not only $^1O_2$ but also $O_2^{\bullet-}$, making it a desirable candidate for treating hypoxic solid tumors. According to the results of *in vivo* and *in vitro* experiments, **Secy5** can efficiently inhibit cancer cell growth *via* anti-Stokes activation processes, thereby providing a novel approach to design anti-Stokes excitation PSs for anticancer treatment.

Photodynamic therapy (PDT) is an emerging therapeutic modality that uses photosensitizers (PSs), light, and O_2 to generate cytotoxic reactive oxygen species (ROS) for anticancer treatment [1–8]. PDT offers several advantages, such as negligible drug resistance, specific spatiotemporal selectivity, and minimal invasiveness [9–15]. Generally, decorating PSs with heavy atom, such as I, S or Se, is a classical approach used to facilitate intersystem crossing (ISC) for enhanced ROS generation. However, limited tissue penetration of visible light due to strong absorption and scattering by tissue components is a significant challenge in PDT research and medicine development [16]. Conversely, near-infrared (NIR) light has emerged as a promising solution for PDT owing to its low photodamage and high penetration [17]. Currently, some efforts have been made to increase the absorption wavelength of PSs by extending the conjugated structures or enhancing the intramolecular charge transfer. However, complex synthesis approaches and poor photo/chemical stability hinder further biomedical applications. To circumvent these troubles, upconversion strategies has been proposed, which can absorb long-wavelength photons and emit short-wavelength photons with a remarkable anti-Stokes shift. Conventional upconversion strategies based on upconversion nanoparticles (UCNPs) or two-photon absorption (TPA) have been proposed to address these issues [18–22]. However, TPA suffers from poor efficiency, thus, high-intensity femtosecond lasers are used [23,24]. Although recently developed UCNPs exhibit enhanced upconversion efficiency, their theoretical photo-upconversion quantum yield remains low because of the high internal energy consumption during multistep energy transfer processes [16,25,26]. The unpredictable systemic toxicity of UCNPs may also lead to biocompatibility and safety concerns [27]. Alternatively, hot band absorption (HBA) may be a promising approach for anti-Stokes excitation PDT. HBA PSs absorb long-wavelength light (anti-Stokes excitation photons) to reach higher excited states by obtaining heat from surrounding to enrich population of the thermal vibrational–rotational state (S_t) of the ground state (S_0) [28,29], then, excited-stated HBA PSs emit short-wavelength light (anti-Stokes fluorescence) or generate ROS through ISC. Unlike TPA and UCNPs that absorb two or

* Corresponding authors.
E-mail addresses: sunwen@dlut.edu.cn (W. Sun), fanjl@dlut.edu.cn (J. Fan).

https://doi.org/10.1016/j.cclet.2024.109631
1001-8417/

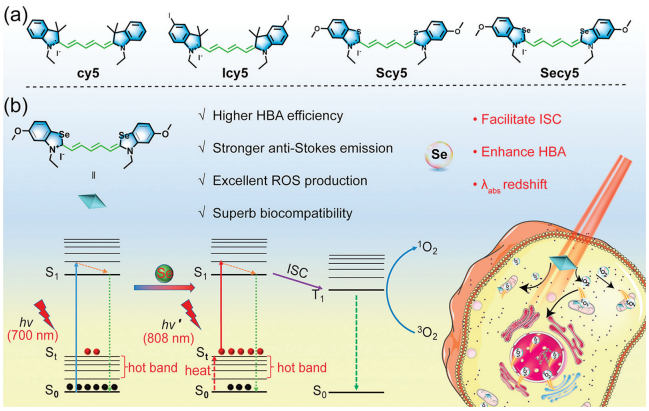

Scheme 1. (a) Chemical structures of **cy5**, **Icy5**, **Scy5**, and **Secy5**. (b) Illustration of **Secy5** for tumor PDT based on HBA.

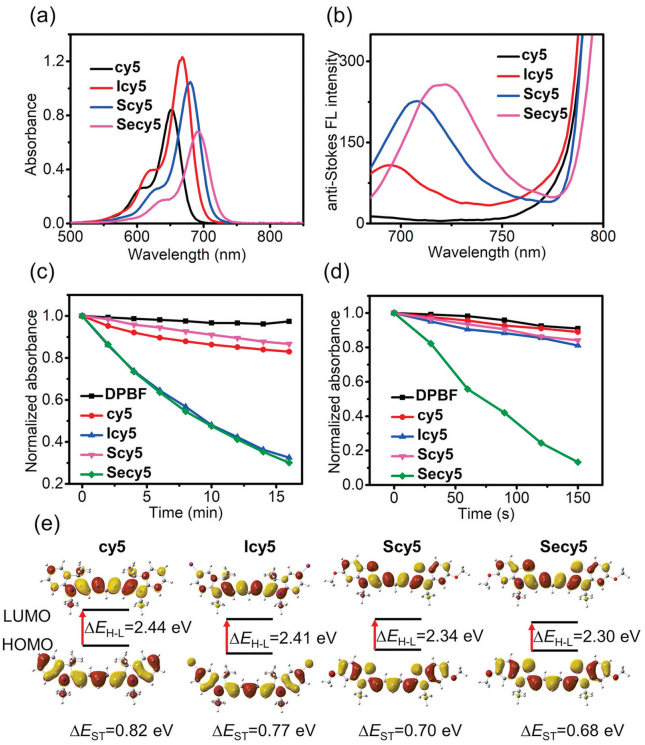

Fig. 1. (a) Absorption spectra of **cy5**, **Icy5**, **Scy5**, and **Secy5** in dichloromethane (DCM), 5 μmol/L. (b) Anti-Stokes fluorescence spectra of **cy5**, **Icy5**, **Scy5**, and **Secy5** (λ_{ex} = 808 nm) in DCM, 5 μmol/L. (c) DPBF degradation induced by **cy5**, **Icy5**, **Scy5**, and **Secy5** (5 μmol/L) under 808 nm light irradiation of different durations in DCM (room temperature). (d) DPBF degradation induced by **cy5**, **Icy5**, **Scy5**, and **Secy5** under 700 nm light irradiation of different durations in DCM (room temperature). (e) The theory model analysis of **cy5**, **Icy5**, **Scy5**, and **Secy5** based on density functional theory.

more photons to reach the excited state, anti-Stokes mediated by HBA is a typical one-photon process, resulting in a lower excitation power density. Therefore, HBA PSs may be much more efficient than TPA and UCNPs, thereby effectively promoting the application of PDT in deeper tissues.

Cyanine dyes are a type of organic fluorophore that has gained considerable attention in biophysics and biochemistry owing to their unique features, such as high extinction coefficient, simple synthetic routes, and excellent biocompatibility [30]. Of these, heptamethine cyanine dyes (Cy7) have been extensively developed for cancer imaging and therapy [31], because the absorption and emission wavelengths of conventional Cy7 are within the 750–800 nm region [32–34]. In addition, indocyanine green (ICG), which has been approved by the Food and Drug Administration (FDA), has a maximum absorption wavelength ($\lambda_{max,\ abs}$) of 785 nm [35,36]. However, ICG suffers from poor photostability severely, which limits its biomedical applications [37]. In contrast, pentamethine cyanine dyes (Cy5) exhibit significantly improved photostability compared with Cy7. Unfortunately, their absorption wavelength cannot reach 750 nm, which is urgently required for biomedical applications [38]. Therefore, developing a strategy to activate Cy5 using near-infrared light of approximately 800 nm is critical for achieving the dual advantages of PSs that can combine long-wavelength excitation and high photostability.

In this study, we synthesized a series of PSs based on Cy5 derivatives, namely, C (**cy5**), I (**Icy5**), S (**Scy5**), and Se (**Secy5**), as illustrated in Scheme 1. Compared with **cy5**, **Icy5**, and **Scy5**, **Secy5** exhibited distinctive advantages, such as higher HBA efficiency, stronger anti-Stokes emission, superb biocompatibility and excellent ROS production under the irradiation of 808 nm light used in clinical practice, thus endowing it with tremendous potential for PDT based on HBA. Although the cyanine platform, **cy5** exhibits much less anti-Stokes fluorescence, enhanced anti-Stokes fluorescence is achieved from **Secy5**, revealing that the synergistic effect of Se and cyanine dyes. And the introduction of methoxy group further extends the excitation wavelength. In addition, excellent ROS production was observed in **Secy5** after light irradiation (Stokes excitation at 700 nm or anti-Stokes excitation at 808 nm), which could be attributed to enhanced ISC, HBA efficiency and better utilization of triplet excited state (T_1). *In vitro* and *in vivo* experiments demonstrated that **Secy5**, as a photosensitizer, can be activated to produce ROS under anti-Stokes excitation, resulting in the elimination of tumor cells and tumors. Therefore, introducing Se into Cy5 for anti-Stokes excitation on HBA is a brilliant strategy for PDT.

Cy5 was chosen as HBA upconversion scaffold because it possesses good photon capture ability and photostability. Hence, we synthesized **Secy5**, with the expectation that it would function as a photosensitizer for anticancer PDT activated by anti-Stokes light. In addition, we synthesized **cy5** (heavy atom-free), **Icy5** (with the classical heavy atom I), and **Scy5** (with the weak heavy atom S) for comparison to demonstrate the HBA capabilities of **Secy5**. As illustrated in Schemes S1 and S2 (Supporting information), ethyl iodide was reacted with 2,3,3-trimethylindolenine, 5-iodo-2,3,3-trimethylindoline, 5-methoxy-2-methylbenzothiazole, and 5-methoxy-2-methylbenzoselenazole, respectively, to produce four quaternary ammonium salts, which were subsequently reacted with *N*-[3-(phenylamino)allylidene]aniline hydrochloride to yield **cy5**, **Icy5**, **Scy5**, and **Secy5**. All the target compounds were fully characterized using ^{1}H NMR, ^{13}C NMR, and ESI-HRMS (Figs. S1–S12 in Supporting information).

Initially, the optical properties of the four PSs were measured and compared. All compounds demonstrated remarkable absorption in the range of 650–750 nm, with molar extinction coefficients (ε) exceeding 1×10^5 L mol^{-1} cm^{-1} (Fig. 1a and Table 1), indicating their exceptional photon capture capability. The $\lambda_{max,\ abs}$ of **Secy5** was 691 nm, which revealed a significant redshift compared with those of **cy5** (39 nm), **Icy5** (23 nm), and **Scy5** (11 nm), suggesting that the incorporation of Se in the Cy5 skeleton could prolong the absorption wavelength, and there is no tail absorption around 808 nm. Remarkably, **Secy5** produced a substantial short-wavelength emission of approximately 720 nm under 808 nm excitation, implying a distinct anti-Stokes process (Fig. 1b). The highest emission peak of **Secy5** under 808 nm excitation was similar to that under 690 nm irradiation (Fig. S13 in Supporting information). This occurrence was also observed in **Icy5** and **Scy5**, but not

Table 1
Photophysical properties of compounds.

Compound	$\lambda_{max,\ abs}$[a] (nm)	$\lambda_{max,\ em}$[b] (nm)	$\lambda_{max,\ em}$[c] (nm)	ε[d] (10^4 L mol^{-1} cm^{-1})	ΔE_{ST}[e] (eV)	SOC[f] (cm^{-1})	τ_F[g] (ns)	Φ_F[h] (%)	τ_T[i] (ns)
cy5	652	675	–[j]	16.5	0.82	0.04	1.25	36.34	9.55
Icy5	668	694	694	22.4	0.77	0.56	1.93	50.25	4.90
Scy5	680	707	707	17.6	0.70	0.12	1.75	43.94	8.30
Secy5	691	720	720	13.6	0.68	0.75	1.49	34.13	3.54

[a] Maximum absorption wavelength in DCM.
[b] Maximum Stokes fluorescence emission wavelength in DCM.
[c] Maximum anti-Stokes fluorescence emission wavelength in DCM.
[d] Molar absorption coefficient (ε is obtained at $\lambda_{max,abs}$).
[e] Energy gap between S_1 and T_1 in DCM.
[f] Spin-orbit coupling constant.
[g] Fluorescence lifetimes in DCM ($\lambda_{ex} = 632$ nm), 5 μmol/L.
[h] Absolute fluorescence quantum yield in DCM (excited by $\lambda_{max,abs}$).
[i] Triplet excited-state lifetime in DCM, 2 μmol/L, N_2.
[j] Not observed.

in **cy5**, suggesting that heavy atoms (I, S, and Se) can confer Cy5 with anti-Stokes fluorescence emission characteristics.

To investigate the capability of these PSs to generate ROS, 1,3-diphenylisobenzofuran (DPBF) was used as a probe to detect singlet oxygen ($^1O_2$) production [39]. Under 808 nm light irradiation, the absorbance of DPBF treated with **Secy5** and **Icy5** at 415 nm decreased gradually, whereas the absorbance changes were barely discernible in the presence of **cy5** and **Scy5** (Fig. 1c and Fig. S14 in Supporting information). **Secy5** exhibited the same $^1O_2$ production ability as that of **Icy5** under 808 nm light irradiation, but outperformed the others under 700, 670, and 650 nm light irradiation (Fig. 1d and Figs. S15–S17 in Supporting information). Meanwhile, singlet oxygen sensor green (SOSG) was also used to detected $^1O_2$, which would emit fluorescence after oxidization by $^1O_2$. As shown in Fig. S18 (Supporting information), under the irradiation of 808 nm light, the fluorescence signal of SOSG fixed with **Secy5** increased gradually, indicating the generation of $^1O_2$. Interestingly, when using SOSG as a probe to detect $^1O_2$ in water, it was found that **Secy5** had a better ability to generate $^1O_2$ than **Icy5**. Besides, $O_2^{\bullet-}$ is also an important member of ROS for killing the tumor cell. Different from energy transfer mechanism of $^1O_2$ generation, $O_2^{\bullet-}$ is generated by electron transfer among PSs in T_1 and molecular oxygen. In addition, the $O_2^{\bullet-}$ generation capability was evaluated using dihydroethidium (DHE) as a specific $O_2^{\bullet-}$ indicator [40]. The fluorescence of DHE was significantly amplified in the presence of **Secy5** (Fig. S19 in Supporting information). The increases in fluorescence intensity of DHE treated with **Secy5** after 10 min irradiation were 5.39 and 5.99 times that of **Scy5** and **Icy5**, respectively. However, the fluorescence intensity of DHE treated with **cy5** demonstrated no obvious change after 10 min irradiation. Thus, these findings clearly demonstrated that the introduction of Se to Cy5 significantly enhanced the generation of ROS.

Density functional theory computation was used to explicate the superior photosensitization capacity of **Secy5**. Fig. 1e and Table 1 show that the singlet–triplet energy gap (ΔE_{ST}) of **Secy5** is the smallest of the four compounds. Generally, a smaller ΔE_{ST} leads to greater ISC efficiency. Although the ΔE_{ST} of **Scy5** was marginally less than that of **Icy5**, the ROS production efficiency of **Icy5** was larger because of spin-orbit coupling (SOC), another significant parameter for ISC efficiency, which also influences ROS production. Greater SOC generally leads to more efficient ISC. The SOC of **Icy5** was much greater than that of **Scy5** (Table 1), thereby demonstrating **Icy5**'s superior $^1O_2$ production ability. Consequently, the lowest ΔE_{ST} and highest SOC could explain the excellent ROS production capability of **Secy5**. The absolute fluorescence quantum yield (Φ_F) could also support the Se-facilitating effect because radiation attenuation competes with the ISC process [41]. The Φ_F (34.13%) of **Secy5** was much lower than that of the others, indicating that **Secy5** in the single excited state (S_1) may dissipate more energy *via* ISC. Furthermore, in comparison to **Icy5** and **Scy5**, the fluorescence lifetime (τ_F) of **Secy5** was also reduced (Fig. S20 in Supporting information). Actually, the introduction of heavy atoms facilitates ISC but does not lead to a decrease in Φ_F and τ_F, as there are three competitive pathways for the dissipation of energy in the S_1. Therefore, it is not sufficient to consider only two of these pathways when discussing energy dissipation. The "heavy atom effect" of Se outperformed those of C, S, and I because the triplet excited-state lifetime (τ_T) of **Secy5** was much shorter than that of the others (Table 1 and Fig. S21 in Supporting information), which was in consistent with quenching of T_1 lifetime caused by "heavy atom effect" [42]. These findings suggest that incorporating Se into PSs would stimulate the highest ISC efficiency.

Cyclic voltammetry was conducted to further investigate redox properties of the cyanines. As shown in Fig. S22a (Supporting information), the degree of anodic shift, reflecting their oxidizing capacity was **Secy5** > **Scy5** > **Icy5** > **cy5**, which was consistent with the ability of their $O_2^{\bullet-}$ generation. The anodic shift of PSs facilitates them to obtain electron, which endows them with potential to perform electron transfer process for type I PDT [43,44]. We then calculated the reduction potentials of their excited states. The excited state reduction potentials of **Secy5**, **Scy5**, **Icy5** and **cy5** were 1.32, 1.31, 1.30 and 1.20 V, also indicating the strongest oxidizing capacity of **Secy5** in excited state. Additionally, type I process also requires the transition to T_1 from S_1. Thus, the lager SOC and lower ΔE_{ST} of **Secy5** than others endowed it with superior ability to generate $O_2^{\bullet-}$.

Scheme 1b shows the mechanism of ISC and anti-Stokes fluorescence, which explains the process of anti-Stokes excitation PDT using HBA. The augmented populations of S_t state using HBA caused PSs to be triggered from S_t to S_1 by anti-Stokes light (808 nm), leading to T_1 *via* ISC for ROS production. According to the Boltzmann distribution, the populations of the hot band depend largely on temperature [28,45]. Thus, temperature-dependent emission and absorption spectra were obtained to validate the regulated HBA anti-Stokes process. With decreasing temperature, the absorbance increased gradually because chromophores tend to be distributed at S_0 at low temperatures (Fig. S23 in Supporting information). On the contrary, high temperature resulted in energy dissipation *via* nonradiative relaxation owing to molecular vibrations and rotations, which resulted in a negative correlation between Stokes fluorescence and temperature (Fig. S24 in Supporting information). In contrast, a positive correlation between the anti-Stokes fluorescence of **Secy5** and temperature was obtained (Fig. S25 in Supporting information), which is consistent with the Boltzmann distribution function prediction. Furthermore, the intensity ratio of the anti-Stokes emission to Stokes emission was used to qualitatively define the relative HBA efficiency [46]. The relative HBA efficiency of **Secy5** was the highest at any temperature (Fig. 2a), and

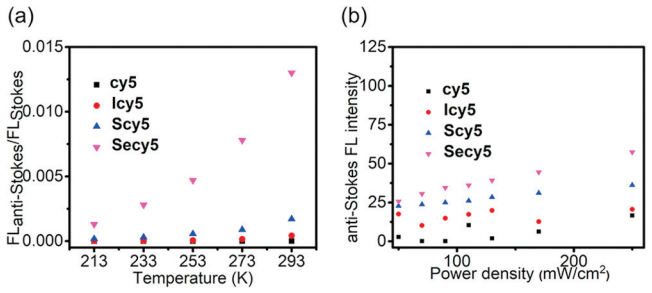

Fig. 2. (a) Relative upconversion efficiencies of **cy5**, **Icy5**, **Scy5**, and **Secy5** (5 μmol/L) at different temperatures (fluorescence intensity ratio between excitation light of 808 nm and that of 670 nm). (b) Anti-Stokes fluorescence changes of **cy5**, **Icy5**, **Scy5**, and **Secy5** (5 μmol/L) irradiated with different laser power intensities (808 nm).

the one-photon absorption upconversion rather than the two or multiphoton absorption process was demonstrated using the linear dependence of anti-Stokes fluorescence intensity on the enhancement of laser power density (Fig. 2b and Fig. S26 in Supporting information). This finding has unparalleled potential in clinical safety. To further explore the function of Se in enhancing HBA, we calculated the activation energy to the thermally populated level (ΔE) [25,47,48]. As shown in Fig. S27 (Supporting information), the ΔE values of the **Icy5**, **Scy5** and **Secy5** are 2.02×10^{-20}, 1.44×10^{-20} and 1.27×10^{-20} J, respectively. And the anti-Stoke fluorescence of **cy5** is not detected at different temperature. The low ΔE value determines **Secy5** is more likely to transition from S_0 to S_t than others. Therefore, Se can enhance HBA through reducing the ΔE value.

Subsequently, a photostability experiment was performed, and as demonstrated in Fig. S28a (Supporting information), the absorbance of **Secy5** remained almost unchanged after a 5 min exposure to 808 nm light, the same property was also observed in **cy5**, **Icy5**, and **Scy5**. Conversely, when exposed to 700 nm light, the absorbance of **Secy5** decreased gradually (Fig. S28b in Supporting information). Furthermore, the absorbance of ICG decreased sharply under 808 nm light irradiation. These findings show that upconversion strategies using HBA are conducive to enhancing photostability as well as the use of PSs in phototherapy.

Considering the exceptional ability of **Secy5** for ROS generation *via* HBA, we investigated its potential application in cellular experiments. Internalization of anticancer agents by tumor cells is a prerequisite for effective treatment. Thus, 4T1 cells were selected and incubated with **Secy5** to demonstrate cellular uptake. After incubating the cells with **Secy5** for 2 h, significant red fluorescence in the 4T1 cells was observed using confocal laser scanning microscopy (Fig. S29 in Supporting information). Furthermore, we assessed the intracellular organelle localization of **Secy5** using commercial organelle-selective trackers, including MitoTracker Green, LysoTracker Green, and Hoechst 33342. MCF-7 cells were co-incubated with **Secy5** and organelle-selective trackers. The red fluorescence of **Secy5** aligned with the green fluorescence of MitoTracker Green (correlation coefficient of 0.912) (Fig. S30 in Supporting information), indicating that **Secy5** was distributed in mitochondria. The correlation coefficients between **Secy5** and Hoechst 33342 and LysoTracker Green were 0.098 and 0.251, respectively. Mitochondria serve as the powerhouses of cells and are essential for energy metabolism and cell survival; hence **Secy5** locating in mitochondria can generate ROS to damage mitochondria and induce cell death, therapy augmenting its potential in anticancer therapy.

The ROS produced by PDT in cancer cells was detected using 2,7-dichlorofluorescein diacetate (DCFH-DA) (Fig. 3) [49]. The cells that were co-incubated with **Secy5** and simultaneously exposed to 808 nm light exhibited green fluorescence, whereas no such fluo-

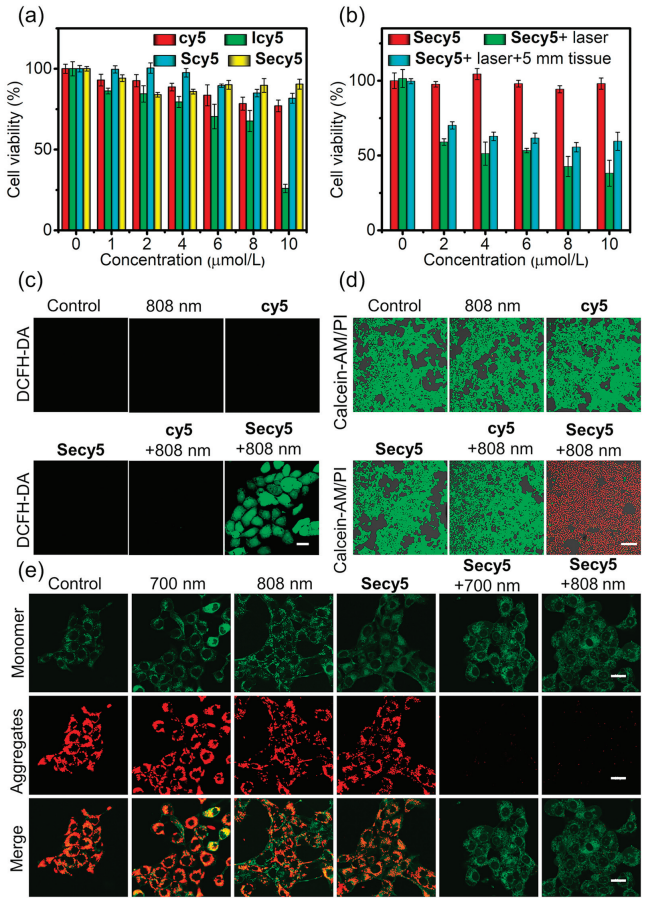

Fig. 3. (a) Viability of 4T1 cells treated with various concentrations of **cy5**, **Icy5**, **Scy5**, and **Secy5** (mean ± SD, $n = 5$). (b) Viability of 4T1 cells treated with different concentrations of **Secy5** under dark or 808 nm light irradiation (300 mW/cm^2, 10 min) (mean ± SD, $n = 3$). (c) Intracellular ROS generation test of **Secy5** (5 μmol/L) under 808 nm light irradiation (300 mW/cm^2, 10 min. Scale bars: 20 μm). (d) Fluorescence images of live/dead cells treated with **Secy5** (5 μmol/L) under 808 nm light irradiation (300 mW/cm^2, 10 min. Scale bars: 200 μm). (e) Mitochondrial membrane potential test for **Secy5** (5 μmol/L)-mediated photodamage of mitochondria (700 nm, 20 mW/cm^2, 10 min; 808 nm, 300 mW/cm^2, 10 min. Scale bars: 20 μm).

rescence was detected in the other treated cells (Fig. 3c). Green fluorescence was also detected in cells treated with **Secy5** and 700 nm light (Fig. S31 in Supporting information). In addition, DHE locating in nucleus was used as a specific probe to detect $O_2^{\bullet -}$, which could bound to DNA and emit red fluorescence after being oxidized by $O_2^{\bullet -}$. After 690 nm light irradiation, red fluorescence in nucleus was observed in 4T1 cells under both normoxia and hypoxia (Fig. S32 in Supporting information). These results demonstrate the production of intracellular ROS by **Secy5** upon irradiation.

To further assess the phototoxicity of **Secy5**, a cell viability assay was performed using the methyl thiazolyltetrazolium (MTT) method. After 12 h of coincubation with PSs, **Secy5** exhibited minimal cytotoxicity to 4T1 cells under dark conditions, whereas **Icy5** showed remarkable cytotoxicity under the identical conditions (Fig. 3a), indicating that **Secy5** possessed better biocompatibility than **Icy5**. After incubation with **Icy5** and **Secy5** for 12 h, the cell viability decreased to approximately 10% and 18%, respectively, under Stokes light (700 nm) irradiation for 8 min (Fig. S33 in Supporting information). However, after incubation with **Icy5** in the absence of light, the cell viability decreased further to approximately 48%, indicating that both the dark toxicity and phototoxicity of **Icy5** were large, and yet its Se-substituted counter-

part (**Secy5**), under the same condition, exhibited good biocompatibility and remarkable phototoxicity. After exposure to anti-Stokes light (808 nm), **Secy5** effectively reduced cell viability in a concentration-dependent manner (Fig. 3b), with a cell viability of approximately 38% after incubation with **Secy5** (10 μmol/L). Furthermore, owing to the efficiency of 808 nm light penetration, **Secy5** inhibited cell proliferation (with a cell viability decrease of approximately 59%) even when the cells were covered with 5 mm thick chicken tissue. This result signifies the significant potential for anti-Stokes excitation PDT based on HBA. As a member of the ROS family, $O_2^{\bullet-}$ can be generated *via* the type I process, which is unaffected by tumor hypoxia microenvironments. Remarkably, **Secy5** can produce $O_2^{\bullet-}$ when exposed to Stokes light, thus enabling PDT in anoxic conditions. Cell viability was dramatically reduced following irradiation with Stokes light under both normoxic and hypoxic conditions (Fig. S34 in Supporting information), which shows **Secy5**'s significant potential for treating hypoxic tumors.

Subsequently, living cells were stained with Calcein-AM, emitting a vibrant green fluorescence, and dead cells were labeled with propidium iodide (PI), emitting a deep red fluorescence. The cells treated with **Secy5** and 808 nm light displayed strong red fluorescence, whereas the control, 808 nm light, and **Secy5** groups exhibited green fluorescence (Fig. 3d). This finding confirms the efficiency of **Secy5** in eliminating 4T1 cells under anti-Stokes excitation. The same phenomenon was also observed in the assay of common Stokes light excitation (Fig. S35 in Supporting information), indicating that **Secy5** is capable of killing cancer cells under both Stokes and anti-Stokes light excitation. To study the cell death mechanism, AnnexinV-FITC/PI were used as the detectors. The AnnexinV can bind to phosphatidylserine which could be everted out of the cytomembrane after cell apoptosis, and present green fluorescence. PI can penetrate cytomembrane of dead cells and bind to nuclear DNA, emitting red fluorescence. The cells treated with **Secy5** and 808 nm irradiation were stained by both green and red fluorescence, indicating that PDT based on HBA induce cell apoptosis and necrosis (Fig. S36 in Supporting information). The mitochondrial damage could be attributed to the disruption of its membrane potential by ROS owing to the localization of **Secy5** in cellular mitochondria. JC-1 was used to evaluate alterations in mitochondrial membrane potential. When the mitochondrial membrane potential is normal, JC-1 forms an aggregate that emits red fluorescence. When the mitochondrial membrane potential is lower, JC-1 exists as a monomer with green fluorescence. PDT triggered by 808 and 700 nm light induced severe mitochondrial depolarization, as inferred from the conspicuous green fluorescence signals (Fig. 3e).

Encouraged by *in vitro* findings, we investigated the potential of **Secy5** for *in vivo* anti-Stokes excitation tumor PDT. All animal experiments were approved by the local research ethics review board of the Animal Ethic Committee of Dalian University of Technology (2019-018). To establish the tumor model, BALB/c mice were subcutaneously injected with 4T1 cells in the right axilla, and the tumors were allowed to grow until their volume reached approximately 100 mm^3. At this point, **Secy5** was injected intratumorally. The intensity of the fluorescence signal increased gradually and reached its maximum after approximately 60 min post-injection (Fig. S37 in Supporting information). Thus, 60 min was considered as the optimal time for irradiation.

To further verify the potential of **Secy5** for anti-Stokes excitation PDT, the mice with tumors were randomly assigned to four groups: (1) Phosphate buffer saline (PBS), (2) **Secy5**, (3) 808 nm laser, and (4) **Secy5** + 808 nm laser. The treatment protocol is illustrated in Fig. S38a (Supporting information). The weight of the mice and the volume of the tumors were measured every other day after different treatments. The tumor growth was not inhibited in the three groups (groups 1, 2, and 3) (Figs. S38b, d and e in Supporting information). After 15 days of treatment, the relative tumor volumes in groups 1, 2, and 3 were about 13, 14, and 14 times the initial tumor size, respectively. In contrast, as anticipated, the tumors in group 4 were significantly inhibited, with a relative tumor volume of approximately 0.4 times the initial tumor size. We also calculated the tumor inhibition rates of four groups to evaluate the therapeutic efficiency of anti-Stokes excitation PDT. As shown in Fig. S39 (Supporting information), the rate of tumor inhibition of group 4 was as high as 95%, while the tumor inhibition rates of other groups were not significant. These excellent results were in accordance with the *in vitro* phototoxicity evaluation, demonstrating the effectiveness of the **Secy5** + 808 nm laser in inhibiting tumor growth.

Preserving the biocompatibility is crucial for the advancement of clinical research. The weight of the mice in each group remained stable throughout the entire treatment duration (Fig. S38c in Supporting information). Furthermore, hematoxylin and eosin (H&E) images of vital organs, such as the heart, liver, spleen, lungs, and kidneys, showed no noticeable physiological damage (Fig. S40 in Supporting information). Therefore, no significant systemic toxicity of **Secy5** to living organisms could be deduced. However, the H&E images of the tumor tissues of mice treated with **Secy5** + 808 nm laser showed visible damage (Fig. S41 in Supporting information). The H&E staining assay revealed that **Secy5** can be used as an anti-Stokes photosensitizer based on HBA for tumor PDT.

In summary, we have reported a photosensitizer based on the HBA strategy, which can be activated by anti-Stokes light (808 nm) *via* a one-photon process to generate ROS for the treatment of tumors. **Secy5**, with its high HBA efficiency, can effectively transit from S_t to excited state S_1 under 808 nm light irradiation because of Se-mediated HBA process. Moreover, the presence of Se significantly narrowed the gap between S_1 and T_1 and improved the SOC, which resulted in higher ISC efficiency for more efficient ROS generation. This improvement was consistent with theoretical calculations. Besides $^1O_2$, under irradiation, **Secy5** also generated $O_2^{\bullet-}$, thereby contributing to the PDT of solid tumors with hypoxic microenvironments. Se substitution of Cy5 ensures not only excellent ROS generation but also tremendous biocompatibility and opens new prospects for treating tumors.

Declaration of competing interest

The authors declare that they have no known competing financial interests or personal relationships that could have appeared to influence the work reported in this paper.

Acknowledgments

This work was financially supported by the National Natural Science Foundation of China (Nos. 21925802, 22022803, 22078046), and the Fundamental Research Funds for the Central Universities (No. DUT22LAB601).

Supplementary materials

Supplementary material associated with this article can be found, in the online version, at doi:10.1016/j.cclet.2024.109631.

References

[1] H.S. Jung, S. Koo, M. Won, et al., Chem. Sci. 14 (2023) 1808–1819.
[2] J. Xie, Y. Wang, W. Choi, et al., Chem. Soc. Rev. 50 (2021) 9152–9201.
[3] Q. Chen, V. Ramu, Y. Aydar, et al., Cancers 12 (2020) 587.
[4] S. Flitsch, C. Duboc, S. Bonnet, JACS Au 2 (2022) 1018–1019.
[5] B. Sun, R. Chang, S. Cao, et al., Angew. Chem. Int. Ed. 59 (2020) 20582–20588.
[6] S. Gao, Y. Jin, K. Ge, et al., Adv. Sci. 6 (2019) 1902137.
[7] Q. Ma, X. Sun, W. Wang, et al., Chin. Chem. Lett. 33 (2022) 1681–1692.
[8] S. Zhou, H. Tian, J. Yan, et al., Chin. Chem. Lett. 35 (2024) 108312.
[9] Z. Li, S. Li, Y. Guo, et al., ACS Nano 15 (2021) 4979–4988.

[10] Y. Cai, D. Ni, W. Cheng, et al., Angew. Chem. Int. Ed. 59 (2020) 14014–14018.
[11] C. Ji, Q. Gao, X. Dong, et al., Angew. Chem. Int. Ed. 57 (2018) 11384–11388.
[12] K.X. Teng, L.Y. Niu, N. Xie, Q.Z. Yang, Nat. Commun. 13 (2022) 6179.
[13] K.X. Teng, L.Y. Niu, Q.Z. Yang, J. Am. Chem. Soc. 145 (2023) 4081–4087.
[14] H. Chen, P. Timashev, Y. Zhang, X. Xue, X.J. Liang, RSC Adv. 12 (2022) 9725–9737.
[15] Z. Liu, J. Zhang, H. Liu, et al., Adv. Mater. 35 (2023) 2208692.
[16] W. Fan, P. Huang, X. Chen, Chem. Soc. Rev. 45 (2016) 6488–6519.
[17] X. Miao, W. Hu, T. He, et al., Chem. Sci. 10 (2019) 3096–3102.
[18] M. Wang, M. Chang, C. Li, et al., Adv. Mater. 34 (2022) 2106010.
[19] H. Chen, B. Ding, P. Ma, J. Lin, Adv. Drug Deliv. Rev. 188 (2022) 114414.
[20] X. Wei, W.B. Cui, G.Y. Qin, et al., J. Med. Chem. 66 (2023) 4167–4178.
[21] J. Xu, L. Xu, C. Wang, et al., ACS Nano 11 (2017) 4463–4474.
[22] H. Liang, X. Liu, Li. Tang, et al., Chin. Chem. Lett. 34 (2023) 107515.
[23] W. Zhao, Y. Zhao, Q. Wang, et al., Small 15 (2019) 1903060.
[24] L. Wu, J. Liu, P. Li, B. Tang, T.D. James, Chem. Soc. Rev. 50 (2021) 702–734.
[25] Y. Liu, Q. Su, X. Zou, et al., Chem. Commun. 52 (2016) 7466–7469.
[26] X. Zhu, Q. Su, W. Feng, F. Li, Chem. Soc. Rev. 46 (2017) 1025–1039.
[27] E.M. Rodrigues, N.D. Calvert, J.C. Crawford, et al., Small 18 (2022) 2107130.
[28] D. Ma, H. Bian, S. Long, et al., Sci. China Chem. 65 (2022) 563–573.
[29] R. Tian, W. Sun, M. Li, et al., Chem. Sci. 10 (2019) 10106–10112.
[30] W. Sun, S. Guo, C. Hu, J. Fan, X. Peng, Chem. Rev. 116 (2016) 7768–7817.
[31] E. Delaey, F. van Laar, D. De Vos, et al., J. Photochem. Photobiol. B Biol. 55 (2000) 27–36.
[32] H.J. Zhou, T.B. Ren, Chem. Asian J. 17 (2022) 202200147.
[33] C. Zhang, L. Long, C. Shi, Adv. Therap. 1 (2018) 1800069.
[34] C. Zhang, T. Liu, Y. Su, et al., Biomaterials 31 (2010) 6612–6617.
[35] J.A. Carr, D. Franke, J.R. Caram, et al., Proc. Natl. Acad. Sci. U. S. A. 115 (2018) 4465–4470.
[36] Y. Xu, J. Yu, J. Hu, et al., Adv. Healthc. Mater. 12 (2023) 2203080.
[37] S. Qi, Y. Wang, Y. Zhu, et al., Nano Today 49 (2023) 101795.
[38] X. Zhao, Q. Yao, S. Long, et al., J. Am. Chem. Soc. 143 (2021) 12345–12354.
[39] W. Liu, H. Gu, B. Ran, et al., Sci. China Mater. 65 (2022) 845–854.
[40] D. Chen, Q. Xu, W. Wang, et al., Small 17 (2021) 2006742.
[41] H. Ma, Y. Lu, Z. Huang, et al., J. Am. Chem. Soc. 144 (2022) 3477–3486.
[42] Z. Wang, A. Toffoletti, Y. Hou, et al., Chem. Sci. 12 (2020) 2829–2840.
[43] J. An, S. Tang, G. Hong, et al., Nat. Commun. 13 (2022) 2225.
[44] K.X. Teng, W.K. Chen, L.Y. Niu, et al., Angew. Chem. Int. Ed. 60 (2021) 19912–19920.
[45] A.V. Kachynski, A.N. Kuzmin, H.E. Pudavar, P.N. Prasad, Appl. Phy. Lett. 87 (2005) 023901.
[46] X. Zhao, S. He, W. Chi, et al., Adv. Sci. 9 (2022) 2202885.
[47] J.L. Clark, P.F. Miller, G. Rumbles, J. Phys. Chem. A 102 (1998) 4428–4437.
[48] R.K. Jain, C. Hu, T.K. Gustafson, S.S. Elliot, M.S. Chang, J. Appl. Phys. 44 (1973) 3157–3161.
[49] H. Xiao, X. Li, B. Li, et al., Small 19 (2023) 2300280.